

# HAM: Hierarchical Attention Model with High Performance for 3D Visual Grounding

Jiaming Chen<sup>†</sup>, Weixin Luo<sup>†</sup>, Xiaolin Wei, Lin Ma<sup>§</sup>, and Wei Zhang<sup>§</sup>

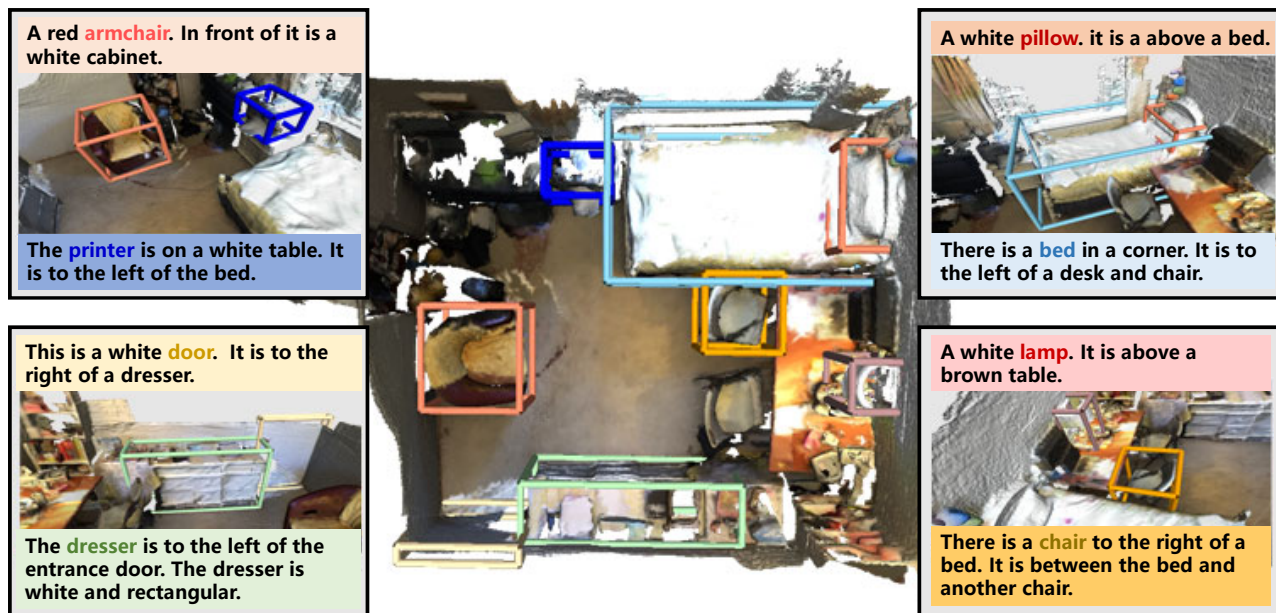


Fig. 1: High performance demonstration of our proposed HAM in ScanRefer Benchmark. One can see that HAM correctly predicts most of the targets (e.g., eight boxes highlighted) in this scene, with more than 50% overlapping with the ground truths.

**Abstract**—This paper tackles an emerging and challenging vision-language task, namely 3D visual grounding on point clouds. Many recent works benefit from Transformer with the well-known attention mechanism, leading to a tremendous breakthrough for this task. However, we find that they realize the achievement by using various pre-training or multi-stage processing. To simplify the pipeline, we carefully investigate 3D visual grounding and summarize three fundamental problems about how to develop an end-to-end model with high performance for this task. To address these problems, we especially introduce a novel Hierarchical Attention Model (HAM), offering multi-granularity representation and efficient augmentation for both given texts and multi-modal visual inputs. Extensive experimental results demonstrate the superiority of our proposed HAM model. Specifically, HAM ranks first on the large-scale ScanRefer challenge, which outperforms all the existing methods by a significant margin. Codes will be released after acceptance.

**Index Terms**—Visual Grounding, Point Clouds, Transformer, Vision-Language

## 1 INTRODUCTION

3D object localization on point clouds using natural language, namely 3D visual grounding, has been a prevailing research topic in multi-modal 3D understanding [1], [2], [3], [4] since the pioneers ScanRefer [1] and ReferIt3D [3] built on subsets of ScanNet [5]. Compared to the well-

studied visual grounding in 2D images [6], [7], [8], 3D visual grounding yet remains unresolved because of more complex 3D relations between objects, visual ambiguity caused by similar indoor furniture, and nonuniform point clouds, etc.

On one hand, existing works [1], [9] usually rely on a Grounding-by-Detection paradigm where an object detector first produces 3D box proposals on observed point clouds, and a visual-linguistic fusion module then locates the target object according to text descriptions. On the other hand, some recent works have already employed the off-the-shelf proposal generator pre-trained by object detection [10], [11] and panoptic segmentation [12] on ScanNet [5]. Different from them, one of our key motivations is to design an end-

J. Chen and W. Luo are the co-first authors. L. Ma and W. Zhang are the corresponding authors.

- J. Chen and W. Zhang are with the School of Control Science and Engineering, Shandong University, China. E-mail: ppjmchen@gmail.com, davidzhang@sdu.edu.cn.
- W. Luo, X. Wei, and L. Ma are with Meituan, China. E-mail: luowx@shanghaiitech.edu.cn, weixiaolin02@meituan.com, forest.linma@gmail.com.

to-end model with high performance for this task. Also, though great progresses [9], [12], [13] have been achieved by introducing powerful transformer [14] with a query-key-value-based attention mechanism, hierarchical modeling on both vision and language inputs has not been fully investigated. However, such an efficient mechanism commonly used in various vision tasks [15], [16], [17] is also much important for 3D visual grounding due to its inherent property, *i.e.*, global and local reasoning, which is another key motivation.

To achieve the above goals, we carefully think about the fundamental problems in 3D visual grounding: i) How to develop an efficient representation for large-scale multi-modal point clouds? First, each scene in the existing benchmarks usually provide coordinates, colors, normal vectors, and multi-view features on average 50,000+ points. Second, the single target object localization in each description is relatively sparse compared to the dense visual inputs. ii) How to abstract complex sentences for grounding? The sentences usually describe complex object relations in physical space globally and locally and indicate visual attributes. iii) How to fuse vision and language features for better grounding? Vision features need to be guided by abstracted language representation to finalize grounding. It should be noticeable that the modulation is much crucial when conducting multi-modalities reasoning.

To answer these questions, we develop a novel Hierarchical Attention Model (HAM) for 3D Visual Grounding on point clouds. In particular, we present its technical novelties corresponding to the above questions. For large-scale multi-modal point representation, we first adopt a hierarchical point abstraction that gradually down-samples the large number of points to a small number of Key-Points and then selects a fewer proposals from these Key-Points. During point abstraction, we propose a simple yet effective redundancy removal strategy *i.e.*, Concentration Sampling (CS) when sampling Key-Points based on their coordinates, colors, and normal vectors, which significantly improves sampling efficiency. Then, a Spatially-Global Attention (SGA) module and a Spatially-Local Attention (SLA) module with a space partition are introduced to guide proposals to globally and locally attend Key-Points, respectively, leading to a hierarchical proposal enhancement in space. As for language representation, we provide word-level and sentence-level embeddings, enabling fine-grained and holistic understanding when processing language data. Since one grounding by one sentence is relatively sparse compared to the auxiliary object detection supervision, we augment sentences by the combination of different sentences within the same scene. Such a language augmentation strategy introduces a balance to these two tasks. Finally, we hierarchically incorporate sentence-level and word-level language features with intermediate Key-Points of detection in both global-level and local-level spaces. Since we incorporate the language into the middle representation rather than the final proposals in detection, HAM performs excellently in both target identification and localization, which achieves the best result of Acc@0.5 on ScanRefer Challenge<sup>1</sup>.

Our contributions are summarized as follows: i) we

introduce a novel end-to-end model which enables hierarchical representation on both vision and language for 3D visual grounding, including efficient point abstraction, multi-granularity linguistic reasoning, and spatially-global and spatially-local attention; ii) we adopt an efficient language augmentation strategy to end-to-end train both detection and grounding in a highly efficient way; iii) HAM without multi-view features, pre-training, or advanced text encoding ranks first on the large-scale ScanRefer challenge, which illustrates the effectiveness of our proposed method.

We organize the rest of the manuscript as below. In Section 2, we list related work, including 2D/3D visual grounding, 3D object detection, *etc.* Section 3 introduces our proposed HAM and demonstrates each module in detail. In Section 4, experiments on two publicly available datasets with extensive ablation studies are carried out to validate the effectiveness of HAM. We summarize this paper in Section 5.

## 2 RELATED WORK

As the most important sub-fields of AI, both computer vision and natural language processing make remarkable progress. Linking two modalities to realize multi-modal artificial intelligence is becoming a new research trend, and a broad range of related tasks has been extended. Most of the Vision-Language tasks can be divided into several main research fields, *e.g.* Vision-Language Understanding [18], [19], [20], [21], [22], Generation [22], [23], [24], [25], [26], Vision-Language and Robotics [27], [28]. This work focus on the emerging and challenging 3D Visual Grounding task, and we further introduce the related work in detail.

### 2.1 Visual Grounding on 2D Images

Visual grounding was first proposed on 2D images, which aims at localizing the target object in an image based on a given sentence query [29], [30], [31], [32]. Most of existing approaches adapt two-stage [8], [33], [34] and one-stage frameworks [35], [36], [37] which are widely used in the object detection. Recently, a set of methods [6], [38] have made great progress in multi-modal understanding tasks, benefiting from the powerful transformer network and large-scale pre-training. Unfortunately, all these methods work on regular 2D images, while they are unable to be directly applied to visual grounding on irregular 3D point clouds.

### 2.2 Visual Grounding on 3D Point Clouds

Visual grounding on 3D point clouds [1], [3] aims at localizing the corresponding 3D bounding box of a target object given query sentences and unorganized point clouds. Two public benchmark datasets *ScanRefer* [1] and *ReferIt3D* [3] are proposed. Both them adopt the *ScanNet* [5], an indoor scene 3D point clouds dataset, and augment it with language annotations. More specifically, *ScanRefer* follows the Grounding-by-Detection paradigm of 2D visual grounding that only raw 3D point clouds and the query sentence are given. Alternatively, *ReferIt3D* formulates the 3D visual grounding as a fine-grained identification problem, which assumes the object ground truth boxes are known

1. [https://kaldir.vc.in.tum.de/scanrefer\\_benchmark](https://kaldir.vc.in.tum.de/scanrefer_benchmark)

during both training and inference. Besides, *Rel3D* [2] is constructed, which focuses on grounding spatial relations between objects but not localization. *SUNRefer* [4] is introduced for visual grounding on RGBD images. In this work, we work on the visual grounding on 3D point clouds only.

To tackle this task, most of existing methods [1], [3], [9], [12], [13], [39], [40] follow the two-stage framework. In the first stage, 3D object proposals are directly generated from the ground-truth [3] or extracted by a 3D object detector [41]. In the second stage, the proposals and language features are aligned for semantic matching. Recent work [9], [13], [42], [43] adopts the popular transformer framework to model the relationship between proposals and language powered by the attention mechanism [14]. Some methods [12], [39], [40] utilize the graph neural network to aggregate information. For instance, TGNN and InstanceRefer [12], [39] treat the proposals as nodes and use language to enhance them. FFL-3DOG [40] characterizes both the proposals and language in two independent graphs and fuses them in another graph. Recently, 3DJCG [44] proposes a unified framework to jointly fit both 3D captioning task and 3D grounding task, which consists of shared task-agnostic modules and task-specific modules. Similarly, D3Net [45] introduces a unified network that can Detect, Describe and Discriminate for both dense captioning and visual grounding in point clouds. 3D-SPS [46] proposes a 3D Single-Stage Referred Point Progressive Selection method for progressively selecting key points with the guidance of language and directly locating the target in a single stage framework. [47] proposes a Multi-View Transformer for 3D visual grounding, which takes the additional multi-view features as inputs and designs the network to learn a more robust multi-modal representation. BUTD-DETR [11] proposes the Bottom Up Top Down Detection Transformers for visual grounding using language guidance and objectness guidance in both 2D and 3D.

Although up-to-date methods on 3D visual grounding have achieved impressive performance, a number of them rely on either a pre-trained proposal generator [11], [12], [39], [45] or extra information such as 2D images [13], [47], and a rule-based language parser [40]. **In this work, we follow the end-to-end Grounding-by-Detection paradigm as ScanRefer [1] and 3DVG-Transformer [9] working on coordinates, colors, and normal vectors of point clouds without any external knowledge.**

### 2.3 3D Object Detection

Since we work on end-to-end 3D visual grounding requiring accurate detection, we then revisit the related work on 3D object detection. To apply CNNs to 3D object detection, early works project the point clouds to the bird’s view [48], [49], [50] or frontal views [51], [52]. Voxel-based methods [53], [54] conduct voxelization on point clouds and utilize 3D and 2D CNNs sequentially as used in 2D object detection. Recently, a bulk of point-based methods [41], [55], [56], [57] put more effort into tackling this task directly on raw point clouds. Most of them group the points into object candidates by using box proposals [55], [56] or voting [41], and then extract object features from groups of points for the following detection. Group-Free [57] drops grounding used in voting [41] and uses K-Closest Point Sampling instead

for proposal generation. At the same time, it applies a transformer to carry out the correlation between proposals and Key-Points, which serves as the foundation of this paper.

More recently, RepSurf-U [58] presents the representative surfaces, a representation of point clouds to explicitly extract the local structure. It provides a lightweight plug-and-play backbone module for downstream tasks containing object detection. Group-Free [57] equipped with RepSurf-U outperforms prior methods. FCAF3D [59], a recently proposed fully convolutional anchor-free framework for object detection in 3D indoor scenes. Different from voting-based and transformer-based methods, it provides an effective and scalable design to manipulate the voxel representation of point clouds with sparse convolutions. FCAF3D achieves the state-of-the-art 3D object detection results on three indoor large-scale 3D point clouds benchmark datasets [5], [60], [61]. In this paper, we adopt point-based detection framework but we believe that voxel-based design is also a strong baseline, which we leave to future work.

### 2.4 Vision-Language Transformer

Transformer-based networks demonstrate extraordinary capability in computer vision [62], [63], [64] and natural language processing [14], [65], [66] and further bridge the gap between them in the multi-modality field [21], [25], [26], [38], [67], which also motivates us to utilize transformer-based framework for our work. Some works [38], [67] conduct large-scale pre-training using a vision-language transformer. For example, CLIP [38] introduces a transformer-based Contrastive Language-Image Pre-training method for efficiently learning visual concepts from natural language supervision. Then TCL [67] proposes Triple Contrastive Learning for vision-language representation pre-training. Besides regular Cross-Modal Alignment (CMA), TCL introduces an Intra-Modal Contrastive (IMC) objective to provide complementary benefits in representation learning. All the network modules, including the vision encoder, text encoder, and fusion encoder, are transformer-based designs. Pre-training with two objectives, *i.e.*, image-text matching and masked language modeling, TCL achieves state-of-the-art performance on various downstream vision-language tasks such as image-text retrieval and visual question answering.

## 3 OUR APPROACH

### 3.1 Overview

In this work, we try to tackle 3D visual grounding with given query sentences and point clouds with 3D coordinates, colors, and normal vectors. To this end, we follow the Grounding-by-Detection paradigm as ScanRefer [1] and 3DVG-Transformer [9] and **intend to design an end-to-end 3D visual grounding network trained from scratch.**

The framework of our proposed method is shown in Figure 2. The raw point clouds and the natural language queries are pre-processed separately for extracting 3D visual proposals and the multi-granularity language embeddings. The two modalities are then fused and interacted in the Spatially-Global Attention (SGA) module and the Spatially-Local Attention (SLA) module. Both SGA and SLA are based

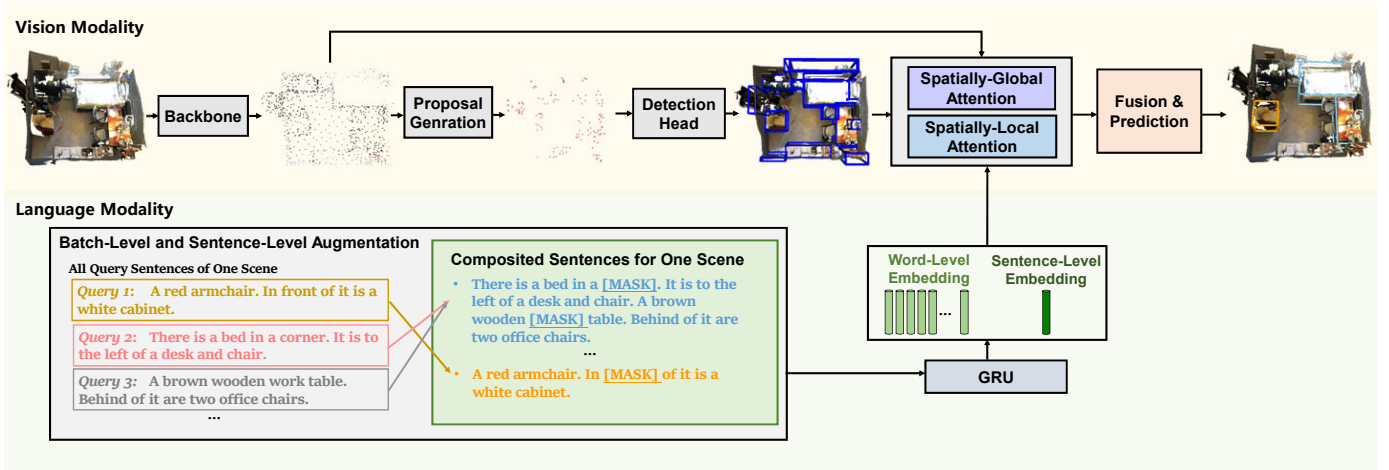


Fig. 2: The pipeline of the proposed HAM. In the Language Modality part, the query sentences of one scene are augmented on both batch-level and sentence-level. In the Vision Modality part, the point clouds are fed into the backbone network based on PointNet++ with a concentration down-sampling strategy. Through the Proposal Generation module and the Detection Module, the Proposal-Points features are extracted to predict the bounding boxes and fuse with the language globally and locally. Finally, the modulated proposals are used to predict the matching scores. Note that we can easily group the proposals into instances by prior object ground truth boxes if applicable, for the sake of ReferIt3D.

on a cross-attention mechanism [14]. The former performs language modulation on proposals in a spatially global field, and the latter finishes the interaction between two modalities in a spatially local field. The modulated proposal features output by these two attention modules is fused and fed into a matching module to predict the matching scores between 3D visual proposals and the query descriptions. The final grounding can be easily realized by selecting the highest matching score.

To better tackle those datasets which convert the grounding to a identification task by offering prior object ground truth boxes annotations, we simply perform late instance grouping by these annotations, while previous works [3], [11], [12], [45] group point clouds by the annotations and then feed them into a PointNet++ [68]. Such a lightweight plugin enables us to better unify our method for all the datasets [1], [3] with different priors.

## 3.2 Language Modality

### 3.2.1 Multi-granularity Language Embedding

In our hierarchical framework, the natural-language input query is embedded in both word-level and sentence-level (“sentence” denotes a single sentence or multiple sentences in query descriptions.), yielding multi-granularity embeddings. Both of them serve as input tokens to be queried in the following point-language attention module of the Spatially-Global Attention and Spatially-Local Attention.

Specifically, for a query text, a pre-trained GloVe [69] model is utilized to extract the initial word embeddings. A vanilla GRU [70] is adopted to extract the **Word-level embedding**  $F_W \in \mathbb{R}^{T \times C}$  for each word token, where the maximum length of texts is set to  $T$ . And then the **Sentence-level embedding**  $F_S \in \mathbb{R}^{1 \times C}$  is the last-step feature of the GRU. In this work, we use simple language embeddings rather than advanced text encoding techniques such as RoBERTa [66], to ensure fair comparisons and ease the end-to-end training.

### 3.2.2 Language Augmentation

Under the basic setting in 3D visual grounding [1], [3], each grounding sample contains a scene from the ScanNet [5] and a reference sentence for one target object with a 3D bounding box. Compared to multiple object detection in one scene, such a grounding setting is much more sparse. Considering that one scene holds dozens of grounding samples, we can easily extend one sentence and one target for one scene to many sentences and many targets for one scene in an individual training sample.

To this end, we adopt two language augmentation strategies to increase the diversity and complexity of the grounding samples during training and to realize a balanced training of grounding and detection. As shown in Figure 2, the first is a sentence-level augmentation following [6] used in the 2D image visual grounding, in which multiple original referential sentences of the same scene are sampled and fused into a composited sentence, which refers to multiple objects in one scene. The second is a batch-level augmentation the same as [9], [45], in which one scene is attached with multiple composited sentences as a single training sample. Thus, we turn the sparse scene grounding task into a dense grounding task, of which effectiveness will be proven in Section 4.4. Further more, following [9], we randomly mask up to 20% words in sentence for robust language modeling.

## 3.3 Vision Modality

### 3.3.1 Visual Backbone with Concentration Sampling

Most of previous methods [1], [9], [12], [13], [40] use PointNet++ [68] as the backbone network for point abstraction when tackling large scale of raw point clouds. In a regular PointNet++, a bulk of Key-Points are sampled through Farthest Point Sampling (FPS). Note that this sampling strategy takes the 3D Euclidean distance of points as the measurement for down-sampling, which is commonly

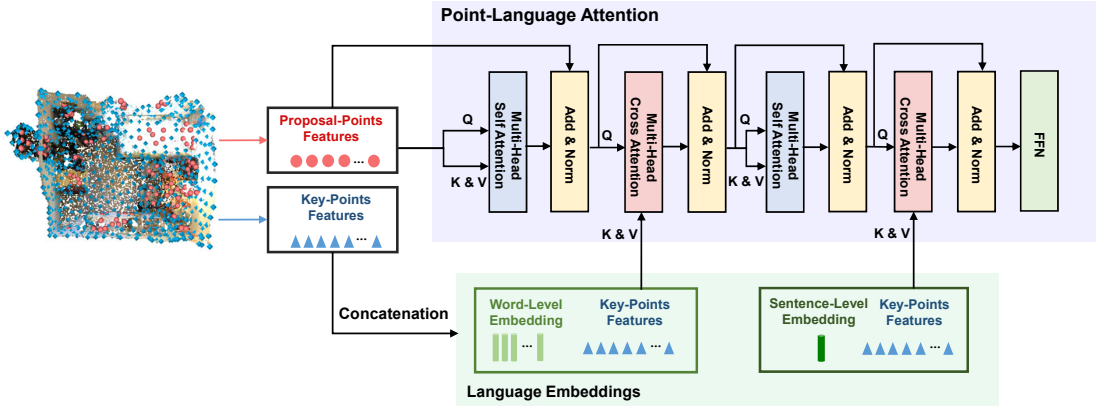


Fig. 3: Point-Language Attention. The Proposal-Points Features serve as query, key, and value in all the Multi-Head Self Attention modules. The Key-Points Features are separately concatenated with the Word-Level Embedding and the Sentence-Level Embedding in the sequence dimension, and they serve as the key and value in the Multi-Head Cross Attention modules.

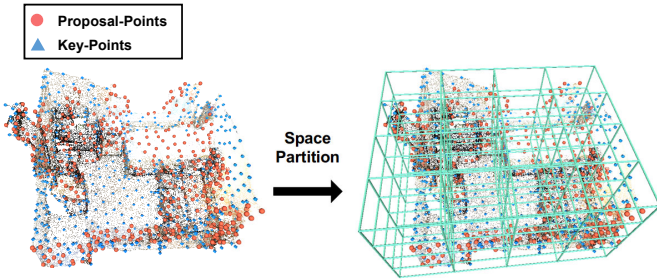


Fig. 4: Space Partition in the Spatially-Local Attention. The scene was partitioned into multiple cubic regions with a resolution of  $4 \times 4 \times 4$ . In the spatially-local attention, the Point-Language Attention is computed on the Proposal-Points and the Key-Points in the same region only.

called Distance-FPS (D-FPS). 3DSSD [71] further proposes a Feature-FPS (F-FPS) strategy, which takes into account the 3D coordinate features extracted by multiple linear layers. To fuse these two samplings, it simply takes 50% D-FPS samples and 50% F-FPS samples, which is called Fusion Sampling (FS). However, there are a significant drawback for FS. The points sampled by F-FPS and D-FPS inevitably will be overlapped without any constraint. Thus, fusing these two sampled sets without redundancy removal will decrease the sampling diversity, leading to a low recall of interested points. In our experiments, we found that the sampling points obtained by FS will cause about 20% overlapped points sampled by both D-FPS and F-FPS.

To remedy these two problems during point abstraction, we proposed a concentration sampling strategy. Specifically, we leverage colors and normal vectors instead of 3D coordinates as additional features for F-FPS, as they are provided in the 3D visual grounding benchmarks [1], [3]. Since colors and normal vectors are dramatically different from the meaning of 3D coordinates, these visual attributes easily help F-FPS discover the salient objects that are usually ignored by D-FPS. Furthermore, using raw colors and normal vectors for F-FPS does not need any additional network-based encoding, which is more computationally efficient

than 3DSSD. To handle the duplicated sampled points by F-FPS and D-FPS, we build up a point-id queue and remove the duplicated point if it is already in the queue. Otherwise, we evenly add sampled points to the queue to ensure 50% points from D-FPS and 50% points from F-FPS without overlapping.

Formally, PointNet++ with concentration sampling efficiently down-samples  $L$  Raw-Points  $P \in \mathbb{R}^{L \times 3}$  with additional visual features  $F \in \mathbb{R}^{L \times (3+3)}$  to  $N$  **Key-Points** denoted as  $P_K = \{P_K^{(i)}\}_{i=1}^N$  with the corresponding features  $F_K \in \mathbb{R}^{N \times C}$ . We also visualize and compare the points sampling by different strategies in the Section 4.5.

### 3.3.2 Proposal Generation

We further utilize the learnable K-Closest Points Sampling (KPS) [57] to select  $M$  **Proposal-Points**  $P_Q = \{P_Q^{(j)}\}_{j=1}^M$  and the corresponding features  $F_Q = \{F_Q^{(j)}\}_{j=1}^M$ . Here both  $F_K$  and  $F_Q$  have the same dimension  $C$ , i.e.,  $F_K \in \mathbb{R}^{N \times C}$  and  $F_Q \in \mathbb{R}^{M \times C}$ .

Inspired by the state-of-the-art 3D object detection performance of Group-Free [57] on ScanNet [5], we follow the Group-Free [57] for the sake of semantic enhancement of Proposal-Points. In particular, multi-head-cross-attention modules are adopted to enhance the Proposal-Points through the correlation with the Key-Points. All these layers are equipped with full supervision by the 3D object detection task on ScanNet. We choose the regressed bounding boxes at the last layer as the boxes of Proposal-Points. In addition, we utilize the 3D box of the Proposal-Point selected by the grounding module as the final localization of the target.

### 3.3.3 Spatially-Global Attention

To finalize grounding on the proposals, we have to fuse vision and language features in an alignment space. Thus, we propose the Point-Language Attention (PLA) based on Multi-Head-Self-Attention (MHSA) and Multi-Head-Cross-Attention (MHCA) [14] also used in the aforementioned semantic enhancement for proposals. As shown in Figure 3,

the word-level features  $F_W$  are concatenated with the Key-Points Features  $F_K$  on the sequence dimension, denoted as  $F_{K,W} \in \mathbb{R}^{(N+T) \times C}$ . The sentence-level feature  $F_T$  is concatenated to the Key-Points Features in the same way, denoted as  $F_{K,T} \in \mathbb{R}^{(N+1) \times C}$ . Formally, we define the MHSA and MHCA as follows:

$$\text{MHSA}(X) = \sigma(f_q(X)f_k(X)^T)f_v(X) \quad (1)$$

$$\text{MHCA}(X, Y) = \sigma(f_q(X)f_k(Y)^T)f_v(Y) \quad (2)$$

Here  $\sigma$  is the softmax function.  $f_q$ ,  $f_k$ , and  $f_v$  are the mapping functions of the query, key, and value, respectively.

Then, for word-level attention, the Proposal-Points Features  $F_P$  are fed into an MHSA layer and an MHCA layer with interaction with  $F_{K,W}$ , formulated as:

$$F_{Q|W} = \text{MHCA}(\text{MHSA}(F_Q), F_{K,W}) \quad (3)$$

Similarly, the sentence-level attention is computed after the word-level attention, formulated as:

$$F_{Q|W,T} = \text{MHCA}(\text{MHSA}(F_{Q|W}), F_{K,T}) \quad (4)$$

Further, a Feed-Forward Network (FFN) including two fully-connect layers is applied on the language-modulated Proposal-Points Features  $F_{Q|W,T}$ . As we perform vision-language modulation at each global scene, we term this operation **Spatially-Global Attention** to distinguish it from the following module.

### 3.3.4 Spatially-Local Attention

The recent Swin-Transformer [15] with window-attention brings locality to the vanilla Transformer [72], which reminds us that the narrations in 3D visual grounding naturally have multiple local descriptions besides a few global ones to localize the target object gradually. For example, ‘‘There a brown cabinet in the kitchen. It is on top of the refrigerator’’ requires the grounder to first localize the ‘‘kitchen’’ in the whole scene and localize the ‘‘brown cabinet’’ in the local space with a reference ‘‘refrigerator’’. Thus, we advocate Spatial Local Attention (SLA) which is parallel to the aforementioned SGA and performs Point-Language Attention locally.

As shown in Figure 4, we partition the whole scene into multiple cubic regions similar to Rubik’s Cube. It yields a low resolution of  $4 \times 4 \times 4$ . Only the Proposal-Points and Key-Points within the same region will conduct PLA locally. For the performance of different partition strategies, we encourage the readers to refer to Section 4.4.

### 3.3.5 Feature Fusion and Prediction

The Spatially-Global Attention and the Spatially-Local Attention are computed in parallel. The former provides the global representations of proposals and the latter provides the local ones. These two language-modulated proposal representation features are simply added together for predicting the matching scores. The matching module is based on a simple MLP network, which predicts the logits of each proposal bounding box. The one with the highest score is the final grounding box.

## 3.4 Objective Functions

We follow the previous work [1], [13], [40] with multi-task training, including 3D object detection, 3D visual grounding and language auxiliary task. Detection plays a critical role in the semantic representation of proposals. At the same time, we believe that this positive-intensive task will significantly benefit the grounding task with a severe imbalance between positives and negatives.

**Detection Loss.** For the detection task, we adopt the same setting with VoteNet [41] and GroupFree [57], where the objectness prediction, box classification, center offset prediction, size classification, and size offset prediction are carried out for each proposal. Here we denote the object detection loss as  $L_D$ .

**Matching Loss.** For the visual grounding, we follow ScanRefer [1] to predict the matching scores  $\{\hat{y}_i\}_{i=1}^M$  of  $M$  Proposal-Points. We set the label  $y_i$  to one only if the box has the highest Interaction-over-Union (IoU) with the ground-truth box, and others are set to zeros. The ground-truth label is a one-hot encoding so we apply Softmax on Matching scores. The cross-entropy loss is utilized as the matching loss function, formulated as:

$$L_M = - \sum_{i=1}^M y_i \log(\hat{y}_i) \quad (5)$$

**Language to object classification loss.** The language description contains the target word, so an auxiliary task of language to object classification can be trained along with the visual grounding to classify the Sentence-Level Feature  $F_T$  to object classes, following ScanRefer [1]. Such classification regularizes the language model, supervised by the cross-entropy loss denoted as  $L_C$ .

**Total Loss.** The total loss  $L$  is a weighted sum of the detection loss, matching loss, and language to object classification loss, denoted as:

$$L = \sum_i w_i * L_i, i \in \{D, M, C\} \quad (6)$$

where the  $w_D, w_M, w_C$  are hyper-parameters to indicate the importance of each task.

## 3.5 Adaptation to Identification Paradigm

The aforementioned framework is designed for the Grounding-by-Detection paradigm as the benchmark method ScanRefer [1] defined. However, another benchmark dataset ReferIt3D [3] introduces the problem of 3D Visual Grounding as an identification task, which provides the object ground truth boxes as known input for both the training and testing stage. Previous works [3], [10], [11], [12] usually group the point clouds of each provided instance at the beginning. However, such pre-processing fails to explore more contexts for point representation at the early stage.

Instead, we provide a simple but effective proposal aggregation mechanism for adapting to the identification setting. For the inputs with extra instance annotation, we retain the raw point clouds as inputs and the detection module. For all the Proposal-Points at the last layer in the detection module, we simply group the Proposal-Points by their instance annotations and adopt max-pooling for

TABLE 1: Comparison with state-of-the-art methods on the ScanRefer [1] benchmark dataset.

Method	Venue	Data	Unique		Multiple		Overall	
			Acc@0.25	Acc@0.5	Acc@0.25	Acc@0.5	Acc@0.25	Acc@0.5
			Validation Set					
ScanRefer [1]	ECCV2020	3D	67.64	46.19	32.06	21.26	38.97	26.10
TGNN [39]	AAAI2021	2D	68.61	56.80	29.84	23.18	37.37	29.70
InstanceRefer [12]	ICCV2021	3D	77.45	66.83	31.27	24.77	40.23	32.93
FFL-3DOG [40]	ICCV2021	3D	-	67.94	-	25.70	-	34.01
3DVG-Transformer [9]	ICCV2021	3D	77.16	58.47	38.38	28.70	45.90	34.47
3DJCG [44]	CVPR2022	3D	78.75	61.30	40.13	30.08	47.62	36.14
3D-SPS [46]	CVPR2022	3D	81.63	64.77	39.48	29.61	47.65	36.43
BUTD-DETR [11]	ECCV2022	3D	-	-	-	-	52.2	39.8
ScanRefer [1]	ECCV2020	2D + 3D	76.33	53.51	32.73	21.11	41.19	27.40
SAT [13]	ICCV2021	2D + 3D	73.21	50.83	37.64	25.16	44.54	30.14
3DVG-Transformer [9]	ICCV2021	2D + 3D	81.93	60.64	39.30	28.42	47.57	34.67
Multi-View Trans [47]	CVPR2022	2D + 3D	77.67	66.45	31.92	25.26	40.80	33.26
3D-SPS [46]	CVPR2022	2D + 3D	<b>84.12</b>	66.72	40.32	29.82	48.82	36.98
3DJCG [44]	CVPR2022	2D + 3D	83.47	64.34	41.39	30.82	<b>49.56</b>	37.33
D3Net [45]	ECCV2022	2D + 3D	-	<b>70.35</b>	-	30.05	-	37.87
<b>HAM</b>		3D	79.24	67.86	<b>41.46</b>	<b>34.03</b>	48.79	<b>40.60</b>
			Online Benchmark					
TGNN [39]	AAAI2021	3D	68.34	58.94	33.12	25.26	41.02	32.81
InstanceRefer [12]	ICCV2021	3D	77.82	66.69	34.57	26.88	44.27	35.80
BUTD-DETR [11]	ECCV2022	3D	<b>78.48</b>	54.99	39.34	24.80	48.11	31.57
ScanRefer [1]	ECCV2020	2D + 3D	68.59	43.53	34.88	20.97	42.44	26.03
3DVG-Transformer [9]	ICCV2021	2D + 3D	77.33	57.87	43.70	31.02	51.24	37.04
3DJCG [44]	CVPR2022	2D + 3D	76.75	60.59	<b>43.89</b>	31.17	<b>51.26</b>	37.76
D3Net [45]	ECCV2022	2D + 3D	-	<b>68.43</b>	-	30.74	-	39.19
<b>HAM</b>		3D	77.99	63.73	41.48	<b>33.24</b>	49.67	<b>40.07</b>

aggregating the Proposal-Instance features. After that,  $M$  Proposal-Points features are aggregated to  $G$  instance features, where  $G$  is the number of instances in the corresponding scene. For the subsequent Spatially-Global Attention and the Spatially-Local Attention, we use the Proposal-Instances features instead of the original Proposal-Points features for finishing the modality fusion and prediction.

## 4 EXPERIMENTS

### 4.1 Implementation Details

For the point clouds, the number of the backbone input points  $L$  is set to 50,000. The number of the Key-Points  $N$  is set to 1,024 and the number of the Proposal-Points  $M$  is set to 512. All of the feature dimension  $C$  is set to 288. The number of the multi-head-cross-attention layers in the proposal generation module is set to 12. For the proposal aggregation, the maximum instance number  $G$  is set to 88. For the sentence-level augmentation, we randomly sample 1 to 6 sentences corresponding to one scene for fusing into the composited sentence. And for the batch-level augmentation, we attach 8 sentences (randomly sampled from the composited and original sentences) to one scene for dense grounding. The maximum sentence length  $T$  is set to 200.

For the positional embedding of all the self-attention and cross-attention layers, following Group-Free [57], the 3D coordinates of the Key-Points are mapped to an positional embedding of the dimension  $C$  via a fully-connected layer and then added to the Key-Point Features. Similarly, the central location and size of the proposal bounding boxes are mapped and added to the Proposal-Points Features. For the word-level features and sentence-level features, we utilize the regular sine-cosine functions as position embedding.

For the region-based Spatially-Local Attention, we provide an efficient implementation based on the mask-attention. Notably, we retain the attention weights of the points in the same region only while others are masked out by filling with infinity before the Softmax operation in the cross-attention layer. Such masked attention can be seamlessly aggregated into Point-Language Attention with high parallelism easily.

Besides, we adopt the AdamW optimizer [73] and set the initial learning rate to  $2 \times 10^{-4}$  for the attention layers and  $1 \times 10^{-2}$  for others. The loss weights  $w_D$ ,  $w_M$ ,  $w_C$  are 10, 0.1 and 0.1. We train the network by 200 epochs, with a batch size of 4. Codes<sup>2</sup> are implemented by Pytorch and run on 8 Tesla-V100 GPUs.

### 4.2 Dataset and Evaluation Metric

ScanRefer [1] and ReferIt3D [3] are two benchmark datasets released recently for visual grounding on point clouds, which are both conducted on the ScanNet [5] dataset but take different evaluation metrics.

**ScanRefer.** It follows the Grounding-by-Detection paradigm as the 2D visual grounding on images that only raw point clouds and query sentences are given. The ScanRefer dataset [1] augments the 3D instance-level indoor dataset ScanNet [5] with 51,583 human-written free-form descriptions of 11,046 objects in 3D scans. It splits the training/validation/testing set with 36,655, 9,508, and 5,410 samples, respectively. We follow the evaluation metric  $Acc@IoU=0.25$  and  $Acc@IoU=0.5$  proposed by ScanRefer to evaluate all the methods. Specifically, they measure the percentage of the positive predicted bounding boxes whose IoUs with the ground-truth bounding boxes are higher than 0.25 and 0.5, respectively. Additionally, scenes with

2. <https://github.com/PPjmchen/HAM>

TABLE 2: Comparison with state-of-the-art methods on the ReferIt3D [3] benchmark dataset.

Subset	Method	Venue	Pre-training	Text Encoder	Data	Overall	Easy	Hard	View-dep.	View-indep.	
Nr3D	ReferIt3D [3]	ECCV2020	✗	RNN [74]	3D	35.6	43.6	27.9	32.5	37.1	
	TGNN [39]	AAAI2021	✗	BERT [65]	3D	37.3	44.2	30.6	35.8	38.0	
	InstanceRefer [12]	ICCV2021	✓	GRU [70]	3D	38.8	46.0	31.8	34.5	41.9	
	3DVG-Transformer [9]	ICCV2021	✗	GRU [70]	3D	40.8	48.5	34.8	34.8	43.7	
	FFL-3DOG [40]	ICCV2021	✗	GRU [70]	3D	41.7	48.2	35.0	37.1	44.7	
	TransRefer3D [42]	ACM MM2021	✗	GRU [70]	3D	42.1	48.5	36.0	36.5	44.9	
	LanguageRefer [43]	CoRL2021	✗	DistilBert [75]	3D	43.9	51.0	36.6	41.7	45.0	
	SAT [13]	ICCV2021	✗	BERT [65]	2D + 3D	49.2	56.3	42.4	46.9	50.4	
	Multi-View Trans [47]	CVPR2022	✓	BERT [65]	2D + 3D	<b>55.1</b>	<b>61.3</b>	<b>49.1</b>	<b>54.3</b>	55.4	
	3D-SPS [46]	CVPR2022	✓	CLIP [38]	2D + 3D	51.5	58.1	45.1	48.0	53.2	
	BUTD-DETR [11]	ECCV2022	✓	RoBERTa [66]	3D	54.6	60.7	48.4	46.0	<b>58.0</b>	
	<b>HAM</b>			✗	GRU [70]	3D	48.2	54.3	41.9	41.5	51.4
Sr3D	ReferIt3D [3]	ECCV2020	✗	RNN [74]	3D	40.8	44.7	31.5	39.2	40.8	
	TGNN [39]	AAAI2021	✗	BERT [65]	3D	45.0	48.5	36.9	45.8	45.0	
	InstanceRefer [12]	ICCV2021	✓	GRU [70]	3D	48.0	51.1	40.5	45.4	48.1	
	3DVG-Transformer [9]	ICCV2021	✗	GRU [70]	3D	51.4	54.2	44.9	44.6	51.7	
	LanguageRefer [43]	CoRL2021	✗	DistilBert [75]	3D	56.0	58.9	49.3	49.2	56.3	
	TransRefer3D [42]	ACM MM2021	✗	GRU [70]	3D	57.4	60.5	50.2	49.9	57.7	
	SAT [13]	ICCV2021	✗	BERT [65]	2D + 3D	57.9	61.2	50.0	49.2	58.3	
	Multi-View Trans [47]	CVPR2022	✓	BERT [65]	2D + 3D	64.5	66.9	58.8	<b>58.4</b>	64.7	
	3D-SPS [46]	CVPR2022	✓	CLIP [38]	2D + 3D	62.6	56.2	<b>65.4</b>	49.2	63.2	
	BUTD-DETR [11]	ECCV2022	✓	RoBERTa [66]	3D	<b>67.0</b>	<b>68.6</b>	63.2	53.0	<b>67.6</b>	
	<b>HAM</b>			✗	GRU [70]	3D	62.5	65.9	54.6	52.5	63.0

TABLE 3: Comparison with state-of-the-art methods on the ReferIt3D Nr3D subset by Acc@0.25 and Acc@0.5. All the results of other methods are provided by the D3Net [45].

Methods	Unique	Multiple	Overall
		Acc@0.5	
ScanRefer [1]	-	12.17	12.17
3DVG-Transformer [9]	-	14.22	14.22
D3Net [45]	-	25.23	25.23
<b>HAM</b>	-	<b>27.11</b>	<b>27.11</b>

a sole target object without similar duplicates are labeled as ‘Unique’ and others as ‘Multiple’ alternatively. Both ‘Unique’ and ‘Multiple’ are unified as ‘Overall’. We report all these evaluation metrics on the validation set and online testing set.

**ReferIt3D.** It contains two sub-datasets, where a sub-dataset is with natural-language reference annotations (*Nr3D*), and another sub-dataset is with synthetic reference annotations (*Sr3D*). *Nr3D* contains 41,503 samples collected by ReferItGame [29], an online reference labeling game on 3D scenes. *Sr3D* contains 83,572 samples collected by a automatic template-based generator. Different from ScanRefer, ReferIt3D casts visual grounding to a identification task and assumes the object ground truth boxes of objects is known during training and inference. During the evaluation, ReferIt3D only needs to calculate the identification accuracy. Similar to ScanRefer, *Nr3D* and *Sr3D* also are further split into different subsets by the sample attributes, where the “easy” and “hard” subsets are defined the same as “Unique” and “Multiple” in ScanRefer, and the “view-dep” and “view-indep” subsets are defined by whether the referring queries are dependent or independent on the camera view. We propose a proposal aggregation strategy for adapting our Grounding-by-Detection framework

to such identification paradigm with the given instance annotations, which is fully introduced in the Section 3.5, and we follow the evaluation metric *Accuracy* proposed by the ReferIt3D [3] to evaluate our method. We also provide *Acc@IoU=0.5* results on ReferIt3D by removing the proposal aggregation following D3Net [45]. Since there is no ‘Unique’ case in ReferIt3D, we report results on ‘Multiple’ and ‘Overall’ subset as D3Net does.

### 4.3 Performance Comparisons with the State-of-the-art Methods

**Quantative Results.** In Table 1 and Table 2, we compare our HAM with the state-of-the-art methods [1], [9], [11], [12], [13], [39], [40], [43], [43], [44], [46], [47] on both ScanRefer [1] and ReferIt3D [3] Nr3D/Sr3D benchmark datasets. For a fair comparison, we report the results according to the modalities used as input data. Here “3D” means only the raw attributes such as coordinates, color, and normal vectors of the raw point clouds are used. “2D + 3D” means using the 2D multi-view features as extra inputs.

Table 1 demonstrates the quantitative results on both the validation set and the online benchmark of the ScanRefer [1]. Surprisingly, HAM only takes the “3D” inputs with efficient end-to-end training and it outperforms all the state-of-the-art methods on the validation set and online benchmark. It is also the champion on the ECCV 2022 ScanRefer Challenge with the highest overall Acc@0.5. For the most challenging metric “Multiple” that expects the grounder to locate the target among multiple objects with the same category, HAM ranks first among all the methods in the validation set for both “Acc@0.25” and “Acc@0.5”, and it also ranks first in the online benchmark for “Multiple Acc@0.5”, which shows its remarkable capacity for 3D visual grounding in complex environments. In addition,

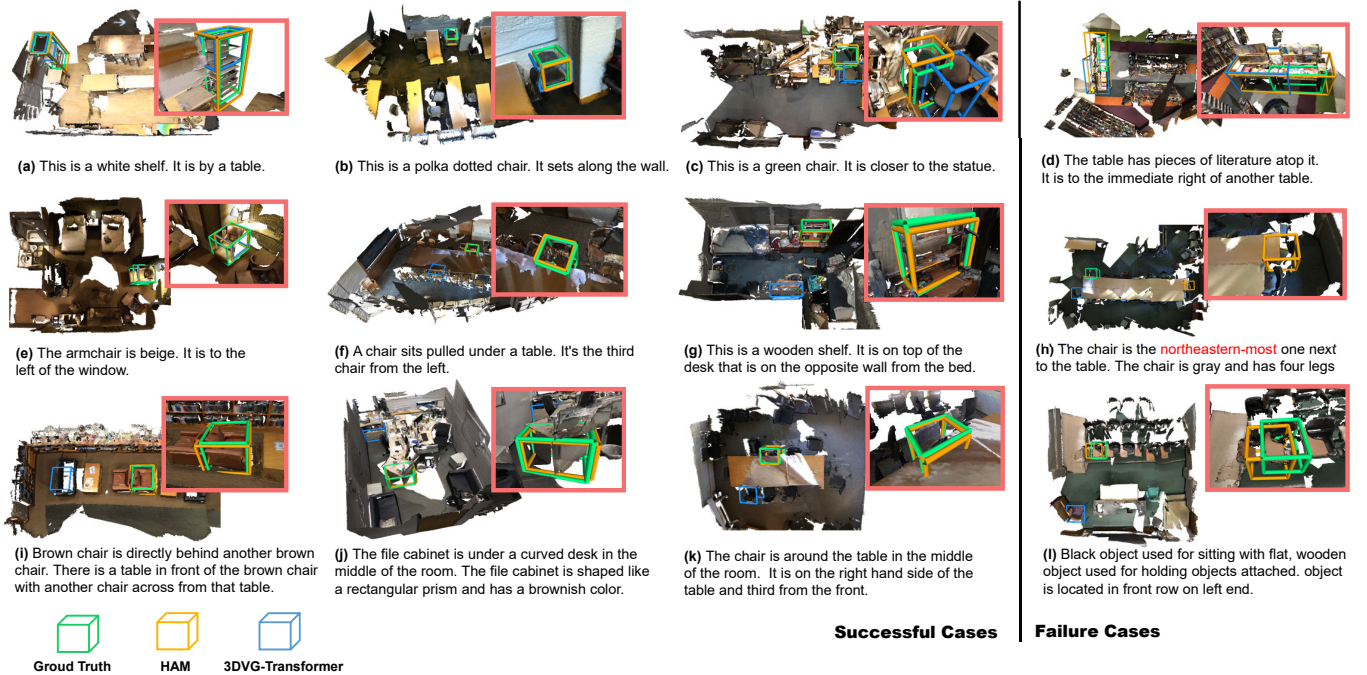


Fig. 5: The visualization results of the proposed method.

without any extra 2D multi-view features and pre-training for the object-detector utilized in a bulk of works [11], [12], [45], our method still has a promising result on “Unique Acc@0.5” compared to D3Net [45].

Table 2 demonstrates the performance on the ReferIt3D [3] Nr3D and Sr3D datasets. HAM demonstrates comparable results, *e.g.*, 48.2% versus SAT (49.2%) on Nr3D and 62.5% versus 3D-SPS (62.6%) on Sr3D. We believe that the given instance priors convert the grounding task to an isolated identification task, leading to a different setting. However, HAM works on the end-to-end 3D visual grounding including localization and identification of the targets. Besides, HAM uses the simple GRU text encoder and does not use any pre-training, compared to others. We also report Acc@0.5 on the ReferIt3D in Table 3. Surprisingly, HAM achieves the best performance again by a significant margin when compared to D3Net ranking second on the more challenging ScanRefer. In summary, we claim that HAM deeply fuses the grounding and detection compared to any previous work who treats detection as a plug-in.

**Qualitative Results.** We visualize several success cases and failure cases of our proposed method as shown in Figure 5. For comparison, we also visualize the predictions of 3DVG-Transformer [9] simultaneously. The results from the first row to the third rows show that HAM well understands texts of various lengths from short to long thanks to the proposed word-level and sentence-level embeddings. Most of the successful cases correctly understand clues from reference objects in texts, for example, ‘by a table’ in Figure 5 (a), ‘closer to the statue’ in Figure 5 (c), and more complex cases such as ‘on the right hand side of the table and third from the front’ in Figure 5 (k). For the “Multiple” samples which require for grounding the target among multiple objects with the same class such as Figure 5 (c)(e)(f)(i)(k), HAM

demonstrates much more excellent discrimination ability, compared to 3DVG-Transformer.

For the failure cases, we summarize three main reasons. The first is the mismatch between text and the scene. For example, in Figure 5 (d), it is difficulty to distinguish two tables in the raw point cloud even for humans. And HAM mistakenly identifies two closely spaced tables as one. The second is the ambiguity from perspective-related description. As shown in Figure 5 (h), the word ‘northeastern-most’ is ambiguous when the perspective is not clear, and HAM predicts the chair on the opposite side of the ground truth box. The third is the incomplete point clouds due to scanning and reconstruction. As shown in Figure 5 (l), the points of the target object are incomplete and it further causes the inaccurate localization of HAM. We believe that alleviating language ambiguity and conducting point cloud completion can significantly contribute to this challenging task, where we leave in future.

#### 4.4 Ablation Studies

In this section, we first conduct an ablation study on ScanRefer [1] for verifying the effectiveness of each component in the proposed HAM. We then carefully ablate the setting of each key component on ScanRefer.

**The ablations on each proposed component.** Here we conduct the ablation experiments for verifying each proposed component. Specifically, as shown on Table 4, the proposed Spatially-Global Attention, Concentration Sampling, Batch-Level Augmentation, Sentence-Level Augmentation, and Spatially-Local Attention are verified and denoted as **SGA**, **CS**, **BL-Aug**, **SL-Aug**, **SLA** for short. For the last three experiments, we also utilize a Stronger Detection Head (**SDH**), which consists of  $l = 12$  (6 by defaults) decoder layers and  $M = 512$  (256 by defaults) Proposal-Points for extracting richer representations and more Proposal-Points.

TABLE 4: The ablation on each proposed component.

Network Setting	Acc@0.25	Acc@0.5
SGA	41.20	32.24
SGA + CS	43.76	34.01
SGA + CS + BL-Aug	45.30	36.47
SGA + CS + BL-Aug + SL-Aug	47.18	38.45
SGA + CS + BL-Aug + SL-Aug + SDH	47.50	40.22
SGA + CS + BL-Aug + SL-Aug + SDH + SLA	<b>47.54</b>	<b>40.66</b>

TABLE 5: The ablations on different down-sampling strategies.

Sampling Strategy	Acc@0.25	Acc@0.5
D-FPS	43.72	32.92
F-FPS	43.24	33.46
FS	42.76	32.40
<b>CS</b>	<b>43.76</b>	<b>34.01</b>

From the experimental results, we find that incrementally stacking each of the proposed modules or strategies of the whole framework brings performance gains gradually on both the Acc@0.25 and the Acc@0.5.

**The Concentration Sampling Strategy.** To explore the effective and efficient sampling strategy for the raw input point clouds with additional features such as colors and normal vectors, we compare our concentration sampling (CS) strategy with the regular Distance Farthest Point Sampling (D-FPS), Feature Farthest Point Sampling (F-FPS) and the Fusion Sampling (FS) [71] on the baseline model. Here we only utilize 6 decoder layers and 256 proposals for detection and the Spatially-Local Attention module is removed (only the Spatially-Global Attention is utilized for vision-language fusion).

As shown in Table 5, taking the colors and normal vectors of the points into account of the down-sampling, the F-FPS gains 0.5% improvement on the Acc@0.5, which means that such additional attribute inputs help filter out more discriminative and meaningful points. However, when utilizing the Fusion Sampling, the performance drops significantly. We believe that a large amount of overlap (around 20%) between the two sampling strategies causes the shortage of high-quality points for the backbone network and the proposal generation. In our concentration sampling setting, the points filtered out by the D-FPS and F-FPS are even without overlapping. Such a simple yet effective strategy achieves the best performance than other down-sampling strategies on both Acc@0.25 and Acc@0.5.

**The Strategies of Language Augmentation.** To further explore the suitable settings for language augmentation, we conduct a series of experiments for both batch-level and sentence-level augmentation.

For the batch-level augmentation which attaches multiple sentences to a single point cloud scene, ablations for the number of the sentences for attaching are conducted. As shown in Table 6, without the sentence-level augmentation, the “8 Sents for BL-Aug” setting performs better than more or fewer sentences. A potential reason is that our framework is trained under the end-to-end Grounding-by-Detection paradigm, so the batch-level augmentation needs to make a trade-off between visual grounding and object detection. When more sentences are associated with a single scene in one training sample batch, the grounding becomes more

TABLE 6: The ablations on language augmentation.

#Sentences for BL-Aug	#Sentences for SL-Aug	Acc@0.25	Acc@0.5
32	1	42.76	32.40
16	1	45.39	35.58
8	1	<b>45.30</b>	<b>36.47</b>
1	1	41.20	32.24
8	[1, 3]	46.63	38.10
8	[1, 6]	<b>47.18</b>	<b>38.45</b>

TABLE 7: The ablations on different partition resolutions for SLA.

Partition Resolution	Acc@0.25	Acc@0.5
without SLA	45.30	36.47
$3 \times 3 \times 3$	47.08	37.87
$4 \times 4 \times 4$	<b>46.42</b>	<b>38.15</b>
$5 \times 5 \times 5$	46.15	36.35

intensive. In summary, a proper number of sentences for batch-level augmentation is significantly important for those Grounding-by-Detection methods including HAM.

For sentence-level augmentation, it provides another enhancement of the raw sentences. We provide two options in Table 6, where [1, 3] and [1, 6] mean that we augment the sentences by a random number from 1 to 3 or from 1 to 6, respectively. The result shows that combining more sentences into a single sentence brings more performance gain.

**The Partition Setting of the Spatially-Local Attention.** We further conduct a series of experiments for exploring the proper partition setting of the SLA. The experimental results are shown in Table 7. We find that compared with the baseline without introducing SLA, both  $3 \times 3 \times 3$  and  $4 \times 4 \times 4$  resolutions achieve better performance. However, when adopting the higher partition resolution  $5 \times 5 \times 5$ , the performance is worse. We assume that though SLA introduces constrained local attention, the number of Key-Points and Proposal-Points in a local region will decrease as the resolution increases. Thus, we use the resolution  $4 \times 4 \times 4$  for the default setting in HAM.

**Different Strategy for Adapting to Identification Paradigm.** We conduct a bulk of experiments on adapting our Grounding-in-Detection HAM framework to the Identification Paradigm for the ReferIt3D [3] dataset, which provides the prior object ground truth boxes for all objects. For simplicity, we adopt the vanilla HAM network without the language augmentation and the Spatially-Local Attention. The detection branch taking the raw point clouds as inputs is retained for providing high-quality Key-Points features for the following point-language attention. A simple yet effective strategy is to assign the predicted bounding box to the object ground truth box with a minimal center distance. Another similar solution is to use the object ground truth boxes that has the maximum Intersection over Union (IoU) with the predicted box as the result. These two strategies only use the object ground truth boxes in the prediction stage without changing any network structure and intermediate features. As shown in Table 8, these two simple strategies achieve comparable performance with some state-of-the-art methods such as TGNN [39] and InstanceRefer [12].

In addition, we try to aggregate all the Proposal-Points within each object ground truth box by mean-pooling or

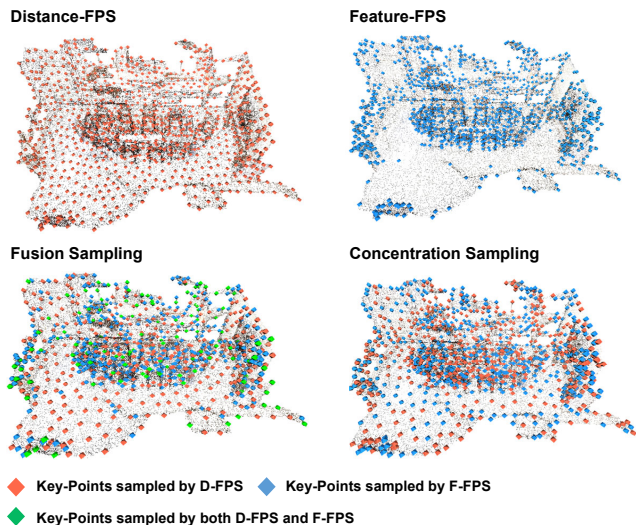


Fig. 6: The visualization of different point sampling strategies. Sampling the same number of points, the concentration sampling not only ensures the coverage of the entire space, but also extracts a sufficient number of high-quality foreground points.

TABLE 8: The ablations on adapting to the identification paradigm (e.g., Nr3D).

Adapting Strategy	Acc@0.25	Acc@0.5	Overall Acc
Center Distance	37.63	27.11	37.90
IoU	37.63	27.11	38.34
Mean-pooling	-	-	42.40
Max-pooling	-	-	43.62

max-pooling on features, as aforementioned in Section 3.5. Then the proposal-level features are converted into instance-level features. We observe a significant performance improvement in Table 8, compared to the assignment strategies with center distance and IoU. We claim that the aggregation from multiple meaningful proposal features act as a voting mechanism.

## 4.5 Visualization

**The visualization of different point sampling strategies.** We visualize the raw point clouds and the 1024 Key-Points filtered out by different sampling strategies as shown in Figure 6. Sampling 1024 Key-Points from the raw point clouds, the Distance-FPS shows an obvious uniform distribution in the whole space because it only considers the coordinates of the points. For the Feature-FPS, it shows a clear aggregation to foreground objects, since it takes the point attributes such as colors and normal vectors into account. Fusion sampling alleviates such unbalance by fusing these two strategies, but it also introduces repeated sampling points, which account for nearly 20% of the total sampling points. Our CS sampling shows that it further extracts a sufficient number of high-quality foreground points by redundancy removal. Also, we only take the additional attributes of the points, *i.e.*, colors and normal vectors as raw features without learning for F-FPS, which is highly efficient.

**The visualization of the weighted Key-Points in SGA and SLA.** As aforementioned in Section 3.3.4, the SGA and SLA

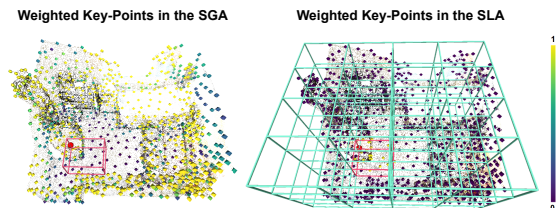


Fig. 7: The visualization of the weighted Key-Points in the Spatially-Global Attention and the Spatially-Local Attention. The Key-Points are highlighted by the normalized attention weights upon the raw point clouds.

are designed for achieving both global and local aggregating in the cross-attention mechanism [14], where the Proposal-Points act as query and the Key-Points and language act as key and value. We visualize the Key-Points weighted by one selected proposal point of both the SGA and SLA on Figure 7, where the selected proposal point is highlighted as a red ball. We find that most of the activated Key-Points are located on the foreground objects of the whole space in the SGA. Such a mechanism encourages the Proposal-Points to accumulate global contexts in space. However, SGA naturally neglects some local points inside the red box. On the contrary, for the SLA, we partition the space into multiple local regions and enforce the Proposal-Points to attend the Key-Points in the same region. It effectively complements local information and enables the model to accumulate global and local contexts.

**The visualization of the Proposal-Points weighted by multi-granularity language representation.** Remind that the proposed point-language attention performs visual-linguistic interaction on both word-level and sentence-level granularities. To demonstrate the effectiveness of such a mechanism, we visualize the Proposal-Points which are attended by such multi-granularity language representation as shown in Figure 8. We can see that the normalized weights of Proposal-Points show obvious regional distribution under different language modulations. The first interesting observation is that the Proposal-Points which are more relevant to the word or the sentence will be assigned a lower attention weight. We assume that such an assignment casts the Proposal-Points into a more discriminative representation space. We also visualize the weights by different words shown on the second column to the fourth column. One can see that not all the words will highlight their corresponding Proposal-Points, for example, “desk” in the first row. We believe using partial words such as “window” is enough to locate the “bed”. For the example in the second row, the target object belongs to the challenging ‘Multiple’ subset. The words “blue”, “chair”, “door” are all activated and it finally grounds the correct “chair” in the scene. And the full sentence always activates the Proposal-Points near the target object. These visualizations demonstrate that HAM can dynamically model discriminative linguistic representation for visual grounding of varying complexity.

## 5 CONCLUSION

In this paper, we investigate the fundamental problems for 3D visual grounding and present a powerful model

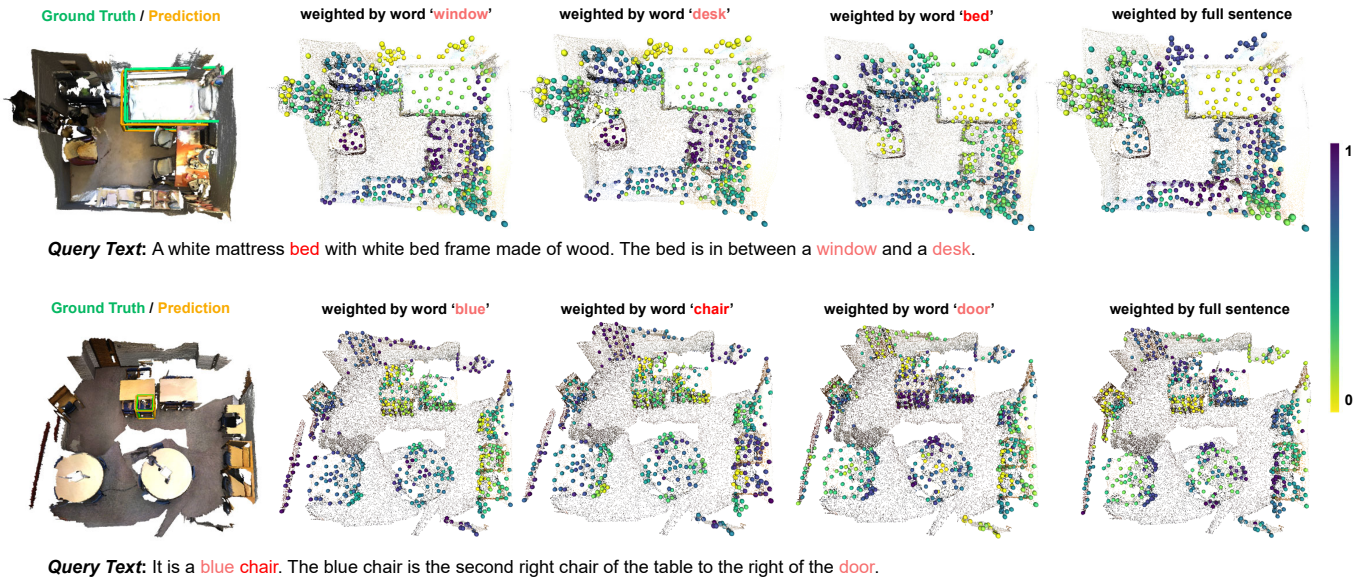


Fig. 8: The visualization of the 512 Proposal-Points which are attended and weighted by the multi-granularity language representation. The Proposal-Points are highlighted by the normalized attention weights upon the raw point clouds.

called HAM. It hierarchically characterizes the vision and language data by providing global and local attention and word-level and sentence-level embeddings, respectively. To stabilize the end-to-end training with target identification and localization, we introduce language augmentation at both batch-level and sentence-level. Our proposed HAM ranks first on the ScanRefer challenge, which significantly outperforms others on both the validation and testing sets. In experiments, we present extensive ablation studies and various visualization to explain how the proposed modules work. We hope that such a simple yet effective model could inspire the research of language on 3D scenes.

## REFERENCES

- [1] D. Z. Chen, A. X. Chang, and M. Nießner, “Scanrefer: 3d object localization in rgb-d scans using natural language,” in *European Conference on Computer Vision*. Springer, 2020, pp. 202–221.
- [2] A. Goyal, K. Yang, D. Yang, and J. Deng, “Rel3d: A minimally contrastive benchmark for grounding spatial relations in 3d,” *Advances in Neural Information Processing Systems*, vol. 33, pp. 10 514–10 525, 2020.
- [3] P. Achlioptas, A. Abdelreheem, F. Xia, M. Elhoseiny, and L. Guibas, “Referit3d: Neural listeners for fine-grained 3d object identification in real-world scenes,” in *European Conference on Computer Vision*. Springer, 2020, pp. 422–440.
- [4] H. Liu, A. Lin, X. Han, L. Yang, Y. Yu, and S. Cui, “Refer-it-in-rgbd: A bottom-up approach for 3d visual grounding in rgbd images,” in *Proceedings of the IEEE/CVF Conference on Computer Vision and Pattern Recognition*, 2021, pp. 6032–6041.
- [5] A. Dai, A. X. Chang, M. Savva, M. Halber, T. Funkhouser, and M. Nießner, “ScanNet: Richly-annotated 3d reconstructions of indoor scenes,” in *Proceedings of the IEEE conference on computer vision and pattern recognition*, 2017, pp. 5828–5839.
- [6] A. Kamath, M. Singh, Y. LeCun, G. Synnaeve, I. Misra, and N. Carion, “Mdet: modulated detection for end-to-end multi-modal understanding,” in *Proceedings of the IEEE/CVF International Conference on Computer Vision*, 2021, pp. 1780–1790.
- [7] J. Deng, Z. Yang, T. Chen, W. Zhou, and H. Li, “Transvg: End-to-end visual grounding with transformers,” in *Proceedings of the IEEE/CVF International Conference on Computer Vision*, 2021, pp. 1769–1779.
- [8] B. A. Plummer, K. Shih, Y. Li, K. Xu, S. Lazebnik, S. Sclaroff, and K. Saenko, “Revisiting image-language networks for open-ended phrase detection,” *IEEE Transactions on Pattern Analysis and Machine Intelligence*, 2020.
- [9] L. Zhao, D. Cai, L. Sheng, and D. Xu, “3dvg-transformer: Relation modeling for visual grounding on point clouds,” in *Proceedings of the IEEE/CVF International Conference on Computer Vision*, 2021, pp. 2928–2937.
- [10] A. Jain, N. Gkanatsios, I. Mediratta, and K. Fragkiadaki, “Looking outside the box to ground language in 3d scenes,” *arXiv preprint arXiv:2112.08879*, 2021.
- [11] —, “Bottom up top down detection transformers for language grounding in images and point clouds,” in *European Conference on Computer Vision (ECCV)*, 2022.
- [12] Z. Yuan, X. Yan, Y. Liao, R. Zhang, S. Wang, Z. Li, and S. Cui, “Instancerefer: Cooperative holistic understanding for visual grounding on point clouds through instance multi-level contextual referring,” in *Proceedings of the IEEE/CVF International Conference on Computer Vision*, 2021, pp. 1791–1800.
- [13] Z. Yang, S. Zhang, L. Wang, and J. Luo, “Sat: 2d semantics assisted training for 3d visual grounding,” in *Proceedings of the IEEE/CVF International Conference on Computer Vision*, 2021, pp. 1856–1866.
- [14] A. Vaswani, N. Shazeer, N. Parmar, J. Uszkoreit, L. Jones, A. N. Gomez, L. Kaiser, and I. Polosukhin, “Attention is all you need,” *Advances in neural information processing systems*, vol. 30, 2017.
- [15] Z. Liu, Y. Lin, Y. Cao, H. Hu, Y. Wei, Z. Zhang, S. Lin, and B. Guo, “Swin transformer: Hierarchical vision transformer using shifted windows,” in *Proceedings of the IEEE/CVF International Conference on Computer Vision*, 2021, pp. 10 012–10 022.
- [16] X. Chu, Z. Tian, Y. Wang, B. Zhang, H. Ren, X. Wei, H. Xia, and C. Shen, “Twins: Revisiting the design of spatial attention in vision transformers,” *Advances in Neural Information Processing Systems*, vol. 34, pp. 9355–9366, 2021.
- [17] Z. Ma, G. Luo, J. Gao, L. Li, Y. Chen, S. Wang, C. Zhang, and W. Hu, “Open-vocabulary one-stage detection with hierarchical visual-language knowledge distillation,” in *Proceedings of the IEEE/CVF Conference on Computer Vision and Pattern Recognition*, 2022, pp. 14 074–14 083.
- [18] S. Antol, A. Agrawal, J. Lu, M. Mitchell, D. Batra, C. L. Zitnick, and D. Parikh, “Vqa: Visual question answering,” in *Proceedings of the IEEE international conference on computer vision*, 2015, pp. 2425–2433.
- [19] Y. Goyal, T. Khot, D. Summers-Stay, D. Batra, and D. Parikh, “Making the v in vqa matter: Elevating the role of image understanding in visual question answering,” in *Proceedings of the IEEE conference on computer vision and pattern recognition*, 2017, pp. 6904–6913.

- [20] A. Das, S. Kottur, K. Gupta, A. Singh, D. Yadav, J. M. Moura, D. Parikh, and D. Batra, "Visual dialog," in *Proceedings of the IEEE conference on computer vision and pattern recognition*, 2017, pp. 326–335.
- [21] J. Chen, W. Luo, W. Zhang, and L. Ma, "Explore inter-contrast between videos via composition for weakly supervised temporal sentence grounding," *Proceedings of the AAAI Conference on Artificial Intelligence*, vol. 36, no. 1, pp. 267–275, Jun. 2022.
- [22] W. Zhang, B. Wang, L. Ma, and W. Liu, "Reconstruct and represent video contents for captioning via reinforcement learning," *IEEE transactions on pattern analysis and machine intelligence*, vol. 42, no. 12, pp. 3088–3101, 2019.
- [23] P. Young, A. Lai, M. Hodosh, and J. Hockenmaier, "From image descriptions to visual denotations: New similarity metrics for semantic inference over event descriptions," *Transactions of the Association for Computational Linguistics*, vol. 2, pp. 67–78, 2014.
- [24] Z. Chen, A. Gholami, M. Nießner, and A. X. Chang, "Scan2cap: Context-aware dense captioning in rgb-d scans," in *Proceedings of the IEEE/CVF Conference on Computer Vision and Pattern Recognition*, 2021, pp. 3193–3203.
- [25] A. Ramesh, M. Pavlov, G. Goh, S. Gray, C. Voss, A. Radford, M. Chen, and I. Sutskever, "Zero-shot text-to-image generation," in *International Conference on Machine Learning*. PMLR, 2021, pp. 8821–8831.
- [26] R. Rombach, A. Blattmann, D. Lorenz, P. Esser, and B. Ommer, "High-resolution image synthesis with latent diffusion models," 2021.
- [27] Y. Qi, Z. Pan, S. Zhang, A. v. d. Hengel, and Q. Wu, "Object-and-action aware model for visual language navigation," in *European Conference on Computer Vision*. Springer, 2020, pp. 303–317.
- [28] A. Das, S. Datta, G. Gkioxari, S. Lee, D. Parikh, and D. Batra, "Embodied question answering," in *Proceedings of the IEEE Conference on Computer Vision and Pattern Recognition*, 2018, pp. 1–10.
- [29] S. Kazemzadeh, V. Ordonez, M. Matten, and T. Berg, "Referitgame: Referring to objects in photographs of natural scenes," in *Proceedings of the 2014 conference on empirical methods in natural language processing (EMNLP)*, 2014, pp. 787–798.
- [30] B. A. Plummer, L. Wang, C. M. Cervantes, J. C. Caicedo, J. Hockenmaier, and S. Lazebnik, "Flickr30k entities: Collecting region-to-phrase correspondences for richer image-to-sentence models," in *Proceedings of the IEEE international conference on computer vision*, 2015, pp. 2641–2649.
- [31] J. Mao, J. Huang, A. Toshev, O. Camburu, A. L. Yuille, and K. Murphy, "Generation and comprehension of unambiguous object descriptions," in *Proceedings of the IEEE conference on computer vision and pattern recognition*, 2016, pp. 11–20.
- [32] L. Yu, P. Poirson, S. Yang, A. C. Berg, and T. L. Berg, "Modeling context in referring expressions," in *European Conference on Computer Vision*. Springer, 2016, pp. 69–85.
- [33] L. Yu, Z. Lin, X. Shen, J. Yang, X. Lu, M. Bansal, and T. L. Berg, "Mattnet: Modular attention network for referring expression comprehension," in *Proceedings of the IEEE Conference on Computer Vision and Pattern Recognition*, 2018, pp. 1307–1315.
- [34] P. Wang, Q. Wu, J. Cao, C. Shen, L. Gao, and A. v. d. Hengel, "Neighbourhood watch: Referring expression comprehension via language-guided graph attention networks," in *Proceedings of the IEEE/CVF Conference on Computer Vision and Pattern Recognition*, 2019, pp. 1960–1968.
- [35] Z. Yang, B. Gong, L. Wang, W. Huang, D. Yu, and J. Luo, "A fast and accurate one-stage approach to visual grounding," in *Proceedings of the IEEE/CVF International Conference on Computer Vision*, 2019, pp. 4683–4693.
- [36] Z. Yang, T. Chen, L. Wang, and J. Luo, "Improving one-stage visual grounding by recursive sub-query construction," in *European Conference on Computer Vision*. Springer, 2020, pp. 387–404.
- [37] B. Huang, D. Lian, W. Luo, and S. Gao, "Look before you leap: Learning landmark features for one-stage visual grounding," in *Proceedings of the IEEE/CVF Conference on Computer Vision and Pattern Recognition*, 2021, pp. 16888–16897.
- [38] A. Radford, J. W. Kim, C. Hallacy, A. Ramesh, G. Goh, S. Agarwal, G. Sastry, A. Askell, P. Mishkin, J. Clark *et al.*, "Learning transferable visual models from natural language supervision," in *International Conference on Machine Learning*. PMLR, 2021, pp. 8748–8763.
- [39] P.-H. Huang, H.-H. Lee, H.-T. Chen, and T.-L. Liu, "Text-guided graph neural networks for referring 3d instance segmentation," in *Proceedings of the AAAI Conference on Artificial Intelligence*, vol. 35, 2021, pp. 1610–1618.
- [40] M. Feng, Z. Li, Q. Li, L. Zhang, X. Zhang, G. Zhu, H. Zhang, Y. Wang, and A. Mian, "Free-form description guided 3d visual graph network for object grounding in point cloud," in *Proceedings of the IEEE/CVF International Conference on Computer Vision*, 2021, pp. 3722–3731.
- [41] C. R. Qi, O. Litany, K. He, and L. J. Guibas, "Deep hough voting for 3d object detection in point clouds," in *proceedings of the IEEE/CVF International Conference on Computer Vision*, 2019, pp. 9277–9286.
- [42] D. He, Y. Zhao, J. Luo, T. Hui, S. Huang, A. Zhang, and S. Liu, "Transrefer3d: Entity-and-relation aware transformer for fine-grained 3d visual grounding," in *Proceedings of the 29th ACM International Conference on Multimedia*, 2021, pp. 2344–2352.
- [43] J. Roh, K. Desingh, A. Farhadi, and D. Fox, "LanguageRefer: Spatial-language model for 3d visual grounding," in *Conference on Robot Learning*. PMLR, 2022, pp. 1046–1056.
- [44] D. Cai, L. Zhao, J. Zhang, L. Sheng, and D. Xu, "3djcg: A unified framework for joint dense captioning and visual grounding on 3d point clouds," in *Proceedings of the IEEE/CVF Conference on Computer Vision and Pattern Recognition*, 2022, pp. 16464–16473.
- [45] D. Z. Chen, Q. Wu, M. Nießner, and A. X. Chang, "D3net: A speaker-listener architecture for semi-supervised dense captioning and visual grounding in rgb-d scans," 2021.
- [46] J. Luo, J. Fu, X. Kong, C. Gao, H. Ren, H. Shen, H. Xia, and S. Liu, "3d-sps: Single-stage 3d visual grounding via referred point progressive selection," in *Proceedings of the IEEE/CVF Conference on Computer Vision and Pattern Recognition*, 2022, pp. 16454–16463.
- [47] S. Huang, Y. Chen, J. Jia, and L. Wang, "Multi-view transformer for 3d visual grounding," in *Proceedings of the IEEE/CVF Conference on Computer Vision and Pattern Recognition*, 2022, pp. 15524–15533.
- [48] J. Ku, M. Mozifian, J. Lee, A. Harakeh, and S. L. Waslander, "Joint 3d proposal generation and object detection from view aggregation," in *2018 IEEE/RSJ International Conference on Intelligent Robots and Systems (IROS)*. IEEE, 2018, pp. 1–8.
- [49] M. Liang, B. Yang, S. Wang, and R. Urtasun, "Deep continuous fusion for multi-sensor 3d object detection," in *Proceedings of the European conference on computer vision (ECCV)*, 2018, pp. 641–656.
- [50] B. Yang, W. Luo, and R. Urtasun, "Pixor: Real-time 3d object detection from point clouds," in *Proceedings of the IEEE conference on Computer Vision and Pattern Recognition*, 2018, pp. 7652–7660.
- [51] X. Chen, H. Ma, J. Wan, B. Li, and T. Xia, "Multi-view 3d object detection network for autonomous driving," in *Proceedings of the IEEE conference on Computer Vision and Pattern Recognition*, 2017, pp. 1907–1915.
- [52] B. Xu and Z. Chen, "Multi-level fusion based 3d object detection from monocular images," in *Proceedings of the IEEE conference on computer vision and pattern recognition*, 2018, pp. 2345–2353.
- [53] S. Song and J. Xiao, "Deep sliding shapes for amodal 3d object detection in rgb-d images," in *Proceedings of the IEEE conference on computer vision and pattern recognition*, 2016, pp. 808–816.
- [54] Y. Zhou and O. Tuzel, "Voxelnet: End-to-end learning for point cloud based 3d object detection," in *Proceedings of the IEEE conference on computer vision and pattern recognition*, 2018, pp. 4490–4499.
- [55] C. R. Qi, W. Liu, C. Wu, H. Su, and L. J. Guibas, "Frustum pointnets for 3d object detection from rgb-d data," in *Proceedings of the IEEE conference on computer vision and pattern recognition*, 2018, pp. 918–927.
- [56] S. Shi, X. Wang, and H. Li, "Pointcrnn: 3d object proposal generation and detection from point cloud," in *Proceedings of the IEEE/CVF conference on computer vision and pattern recognition*, 2019, pp. 770–779.
- [57] Z. Liu, Z. Zhang, Y. Cao, H. Hu, and X. Tong, "Group-free 3d object detection via transformers," in *Proceedings of the IEEE/CVF International Conference on Computer Vision*, 2021, pp. 2949–2958.
- [58] H. Ran, J. Liu, and C. Wang, "Surface representation for point clouds," in *Proceedings of the IEEE/CVF Conference on Computer Vision and Pattern Recognition*, 2022, pp. 18942–18952.
- [59] D. Rukhovich, A. Vorontsova, and A. Konushin, "Fcaf3d: Fully convolutional anchor-free 3d object detection," *arXiv preprint arXiv:2112.00322*, 2021.
- [60] S. Song, S. P. Lichtenberg, and J. Xiao, "Sun rgb-d: A rgb-d scene understanding benchmark suite," in *Proceedings of the IEEE conference on computer vision and pattern recognition*, 2015, pp. 567–576.
- [61] I. Armeni, O. Sener, A. R. Zamir, H. Jiang, I. Brilakis, M. Fischer, and S. Savarese, "3d semantic parsing of large-scale indoor

- spaces," in *Proceedings of the IEEE conference on computer vision and pattern recognition*, 2016, pp. 1534–1543.
- [62] D. Lian, D. Zhou, J. Feng, and X. Wang, "Scaling & shifting your features: A new baseline for efficient model tuning," in *Advances in Neural Information Processing Systems (NeurIPS)*, 2022.
- [63] S. Cao, W. Luo, B. Wang, W. Zhang, and L. Ma, "A circular window-based cascade transformer for online action detection," *arXiv preprint arXiv:2208.14209*, 2022.
- [64] Y. Qian, W. Luo, D. Lian, X. Tang, P. Zhao, and S. Gao, "Svip: Sequence verification for procedures in videos," in *Proceedings of the IEEE/CVF Conference on Computer Vision and Pattern Recognition*, 2022, pp. 19 890–19 902.
- [65] J. Devlin, M.-W. Chang, K. Lee, and K. Toutanova, "Bert: Pre-training of deep bidirectional transformers for language understanding," *arXiv preprint arXiv:1810.04805*, 2018.
- [66] Y. Liu, M. Ott, N. Goyal, J. Du, M. Joshi, D. Chen, O. Levy, M. Lewis, L. Zettlemoyer, and V. Stoyanov, "Roberta: A robustly optimized bert pretraining approach," *arXiv preprint arXiv:1907.11692*, 2019.
- [67] J. Yang, J. Duan, S. Tran, Y. Xu, S. Chanda, L. Chen, B. Zeng, T. Chilimbi, and J. Huang, "Vision-language pre-training with triple contrastive learning," in *Proceedings of the IEEE/CVF Conference on Computer Vision and Pattern Recognition*, 2022, pp. 15 671–15 680.
- [68] C. R. Qi, L. Yi, H. Su, and L. J. Guibas, "Pointnet++: Deep hierarchical feature learning on point sets in a metric space," *Advances in neural information processing systems*, vol. 30, 2017.
- [69] J. Pennington, R. Socher, and C. D. Manning, "Glove: Global vectors for word representation," in *Proceedings of the 2014 conference on empirical methods in natural language processing (EMNLP)*, 2014, pp. 1532–1543.
- [70] J. Chung, C. Gulcehre, K. Cho, and Y. Bengio, "Empirical evaluation of gated recurrent neural networks on sequence modeling," *arXiv preprint arXiv:1412.3555*, 2014.
- [71] Z. Yang, Y. Sun, S. Liu, and J. Jia, "3dssd: Point-based 3d single stage object detector," in *Proceedings of the IEEE/CVF conference on computer vision and pattern recognition*, 2020, pp. 11 040–11 048.
- [72] A. Dosovitskiy, L. Beyer, A. Kolesnikov, D. Weissenborn, X. Zhai, T. Unterthiner, M. Dehghani, M. Minderer, G. Heigold, S. Gelly, J. Uszkoreit, and N. Houlsby, "An image is worth 16x16 words: Transformers for image recognition at scale," 2021.
- [73] I. Loshchilov and F. Hutter, "Decoupled weight decay regularization," *arXiv preprint arXiv:1711.05101*, 2017.
- [74] S. Hochreiter and J. Schmidhuber, "Long short-term memory," *Neural computation*, vol. 9, no. 8, pp. 1735–1780, 1997.
- [75] V. Sanh, L. Debut, J. Chaumond, and T. Wolf, "Distilbert, a distilled version of bert: smaller, faster, cheaper and lighter," *arXiv preprint arXiv:1910.01108*, 2019.